AIAA JOURNAL
Vol. 44, No. 8, August 2006

Nonlinear Reduced Order Random Response Analysis of Structures with Shallow Curvature

Adam Przekop*
National Institute of Aerospace, Hampton, Virginia 23666
and
Stephen A. Rizzi†
NASA Langley Research Center, Hampton, Virginia 23681

DOI: 10.2514/1.18868

The goal of this investigation is to further develop nonlinear modal numerical simulation methods for application to geometrically nonlinear response of structures with shallow curvature under random loadings. For reduced order analysis, the modal basis selection must be capable of reflecting the coupling in both the linear and nonlinear stiffness. For the symmetric shallow arch under consideration, four categories of modal basis functions are defined. Modal bases having symmetric transverse displacements and modal bases having anti-symmetric transverse displacements may each be either transverse dominated or in-plane dominated. The response of an aluminum arch under a uniformly distributed transverse random loading is investigated. Results from nonlinear modal simulations made using various modal bases are compared with those obtained from a numerical simulation in physical degrees-of-freedom. While inclusion of transverse dominated modes having a symmetric transverse displacement is important for all response regimes, it is found that the in-plane dominated modes having a symmetric transverse displacement become increasingly important in the nonlinear response regime. In the autoparametric response regime, the inclusion of both transverse and in-plane dominated modes, each with an anti-symmetric transverse displacement distribution, is found to be critical.

Nomenclature

$\boldsymbol{C}, \tilde{\boldsymbol{C}}$	=	proportional damping matrix (physical and modal coordinates)
d, a, b	=	linear, quadratic nonlinear, and cubic nonlinear modal stiffness coefficients
$\boldsymbol{F}, \tilde{\boldsymbol{F}}$	=	force excitation vector (physical and modal coordinates)
$\boldsymbol{F}_{NL}, \tilde{\boldsymbol{F}}_{NL}$	=	nonlinear restoring force (physical and modal coordinates)
$\boldsymbol{K}, \tilde{\boldsymbol{K}}$	=	linear stiffness matrix (physical and modal coordinates)
$\boldsymbol{M}, \tilde{\boldsymbol{M}}$	=	mass matrix (physical and modal coordinates)
t	=	time
u, v, ϕ	=	horizontal and vertical displacement, and rotation (global physical coordinates)
$\boldsymbol{X}, \boldsymbol{q}$	=	displacement response vector (physical and modal coordinates)
$\boldsymbol{\Phi}$	=	modal basis function matrix
ζ	=	viscous damping factor
ω	=	undamped natural frequencies
$\lceil \boldsymbol{I} \rfloor$	=	identity matrix

I. Introduction

DIRECT numerical simulation of nonlinear random response in physical degrees-of-freedom (DoFs) is computationally intensive for even the simplest structures. Its use for design of high-cycle-fatigue tolerant aerospace vehicle structures is considered impractical. Accordingly, much effort has been spent in recent years to develop accurate reduced order analyses, such as finite element-based nonlinear modal numerical simulation, which could be suitable for use in design environments.

Reduced order finite element methods may be viewed as being in one of two categories; those in which the nonlinear modal stiffness is directly evaluated from the nonlinear finite element stiffness matrix (so-called direct methods), and those in which the nonlinear modal stiffness is indirectly evaluated. Direct methods are typically implemented in special purpose finite element codes in which the nonlinear stiffness is known [1–4]. The only known implementation of a direct method in a commercial code is due to Bathe and Gracewski [5]. Indirect stiffness evaluation methods are typically implemented for use with commercial finite element codes in which the nonlinear stiffness is unavailable [6,7]. In the indirect method used in this paper, a series of prescribed displacement fields is formed from combinations of basis functions. Using a finite element static nonlinear solution, nonlinear restoring forces corresponding to these displacement fields are obtained and are used to compute linear and nonlinear modal stiffness coefficients. For both direct and indirect stiffness evaluation approaches, the accuracy of the solution depends on the selection of the modal basis, through which the nonlinear modal stiffness may be determined. The majority of research performed in the field of reduced order numerical simulation of thin-walled aerospace structures has been primarily focused on isotropic planar configurations [1,7–12]. Through comparison with numerical simulation in physical DoFs, the authors recently demonstrated the ability of a reduced order method to accurately predict geometrically nonlinear random displacement and stress response for planar isotropic structures, provided that a suitable modal basis is utilized [8]. However, most practical aerospace applications involve more complex geometries. Thus, the focus of this study is to extend the authors' previous work using an indirect stiffness evaluation approach to determine the effect of modal basis selection on the response of structures with shallow curvature. It is known that such structures may exhibit not only a hardening but also a softening type of nonlinearity [13,14] which may be nonconservative relative to a linear solution.

For planar configurations, the linear bending and membrane responses are uncoupled. Only the large deflection nonlinear

Presented as Paper 2260 at The 46th AIAA/ASME/ASCE/AHS Structures, Structural Dynamics, and Materials Conference, Austin, TX, 18–21 April 2005; received 15 July 2005; accepted for publication 1 January 2006.

*Research Scientist, AIAA Senior Member.
†Aerospace Engineer, Structural Acoustics Branch, AIAA Associate Fellow.

response couples the bending and membrane behavior. Therefore, basis functions derived from a linear eigenanalysis are readily separable into eigenvectors associated with only the bending response and those associated with only the membrane response. Curved structures, on the other hand, exhibit an inherent linear coupling between transverse and in-plane (membrane) displacements. This coupling is independent of the response magnitude. Similar to the planar configuration, there also exists a coupling of transverse and in-plane displacements resulting from large deflection nonlinearity. Therefore, for reduced order analysis, the modal basis selection must be capable of reflecting the coupling in both the linear and nonlinear stiffness. For the structures under consideration, two categories of modes are defined. Those having symmetric transverse displacements, with antisymmetric rotations and in-plane displacements, are subsequently referred to as ST modes. Those having antisymmetric transverse displacements, with symmetric rotations and in-plane displacements, are referred to as AT modes. The ST and AT modes may be further classified according to their dominant behaviors. Mass-normalized eigenvectors dominated by the transverse component will be referred to as a type T mode and those dominated by the in-plane component will be referred to as a type I mode. Consequently, this study is limited to shallow curvatures, allowing the identification of basis functions that are either type T or type I. For the structure considered, type T modes typically have lower natural frequencies than type I modes. Hence, four classes of modes are considered for inclusion in the modal basis, i.e., ST-T, ST-I, AT-T, and AT-I.

The presence of nonlinear coupling also implies a possibility of autoparametric resonance [15], which is also referred to as autoparametric interaction, and is one possible form of internal resonance [16]. While it is possible to construct a linear system exhibiting internal resonance, the problems of interest here are those in which the resonance is due to geometric nonlinearity. An external loading can *directly* excite only a motion which is consistent with its characteristics, i.e., symmetric loading acting on a symmetric structure directly excites a symmetric transverse and antisymmetric in-plane response. However, if sufficiently high nonlinear modal interactions exist, a response behavior not conforming to an external loading may also be initiated [17]. In other words, an energy flow can occur from a *primary* system, which is subject to an external excitation, into a *secondary* system, which is not subject to an external excitation. Once the secondary system is excited, the energy flow occurs in both directions [18]. The energy flowing back from the secondary to the primary system in conjunction with a viscous damping can cause the secondary system response to exhibit an intermittent behavior.

An aluminum arch with shallow curvature under transverse loading is considered. Comparisons between nonlinear modal simulations and numerical simulations in physical DoFs are made to determine the proper modal basis selection. Of particular interest is the condition of autoparametric resonance and its effect on the required basis selection.

II. Nonlinear Numerical Simulation in Physical DoFs

The shallow arch with cylindrical curvature was first analyzed with numerical simulation in physical DoFs to give an insight into the characteristic behavior of nonplanar structures. In this respect, the simulation is treated as if it were an experimental observation. It will therefore help guide the selection of basis functions used in the reduced order nonlinear modal simulation, and will ultimately be used to validate those results. A clamped-clamped aluminum arch measuring $18 \times 1 \times 0.09$ in. (projected length $\times$ width $\times$ thickness) and 81.25 in. radius of curvature was considered, as shown in Fig. 1. This geometry gave a radius/span ratio of approximately 4.5. The following material properties were used:

$$E = 10.6 \times 10^6 \text{ psi}, \qquad G = 4.0 \times 10^6 \text{ psi},$$

$$\rho = 2.588 \times 10^{-4} \frac{\text{lb}_f - \text{s}^2}{\text{in}^4}$$

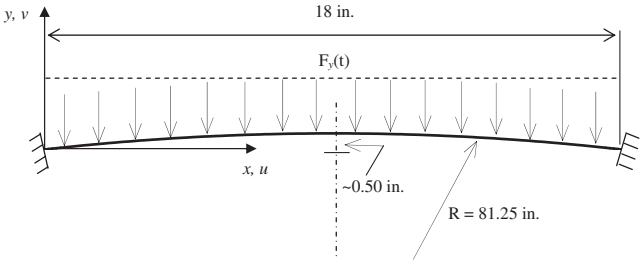

Fig. 1 Geometry of shallow arch.

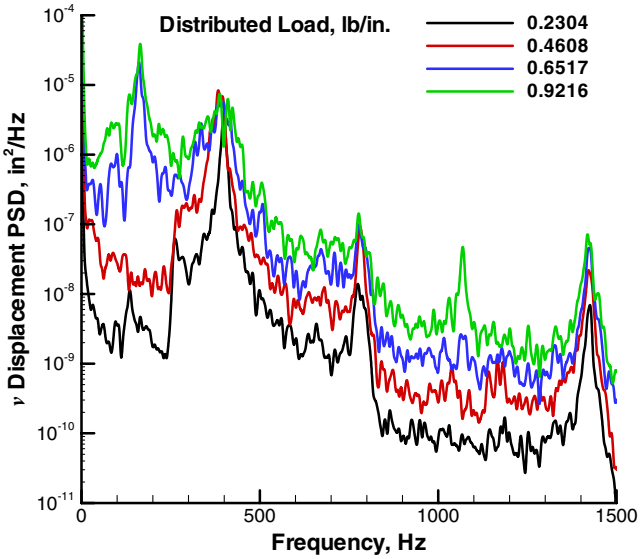

Fig. 2 Vertical displacement PSD at quarterspan location.

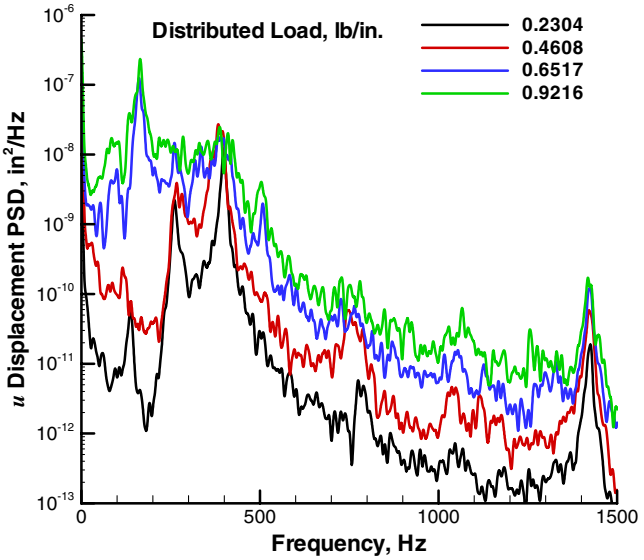

Fig. 3 Horizontal displacement PSD at quarterspan location.

Mass proportional damping was specified corresponding to critical damping of 2.0% for the first symmetric transverse mode (at 258 Hz). A random load generation process previously presented [9] was applied, giving a flat excitation spectrum from 0 to 1500 Hz. The arch was uniformly loaded along its span in the vertical direction, irrespective of the deformation, i.e., follower forces were not utilized.

The finite element program ABAQUS (version 6.5-1) was used to generate nonlinear displacement time histories. The double precision explicit integration scheme with an automatic time integration step selection, referred to as "element by element" in ABAQUS, was

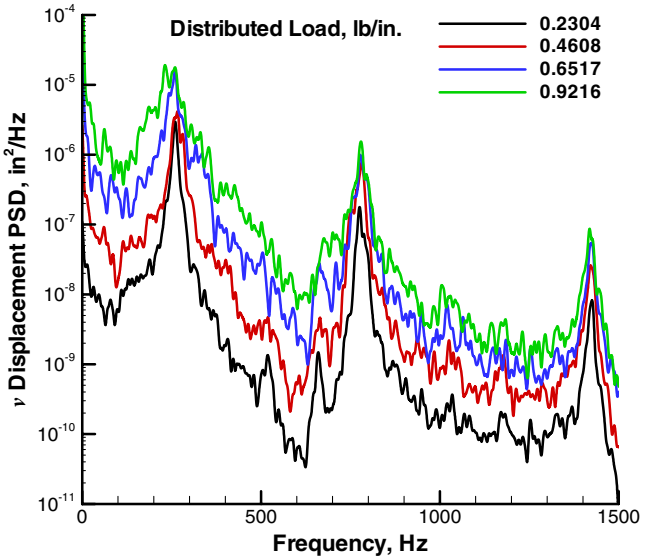

Fig. 4 Vertical displacement PSD at midspan location.

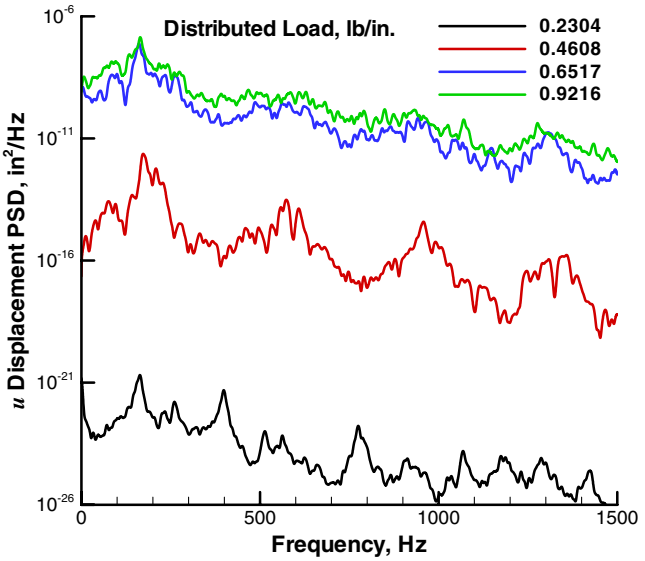

Fig. 5 Horizontal displacement PSD at midspan location.

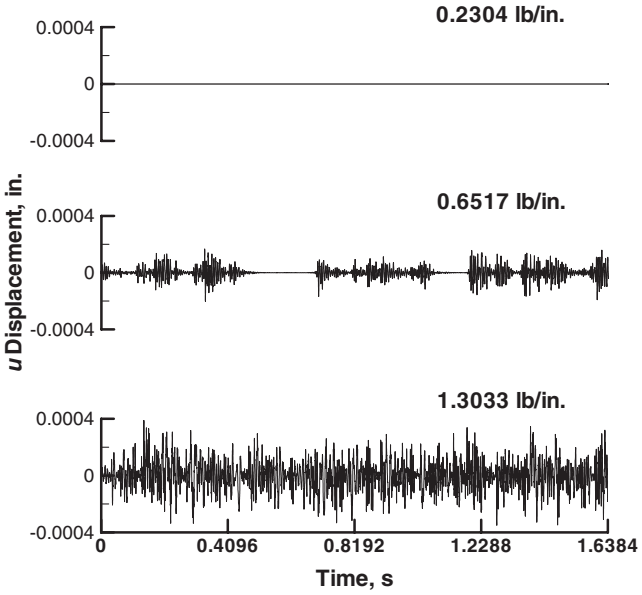

Fig. 6 Midspan horizontal displacement response time histories.

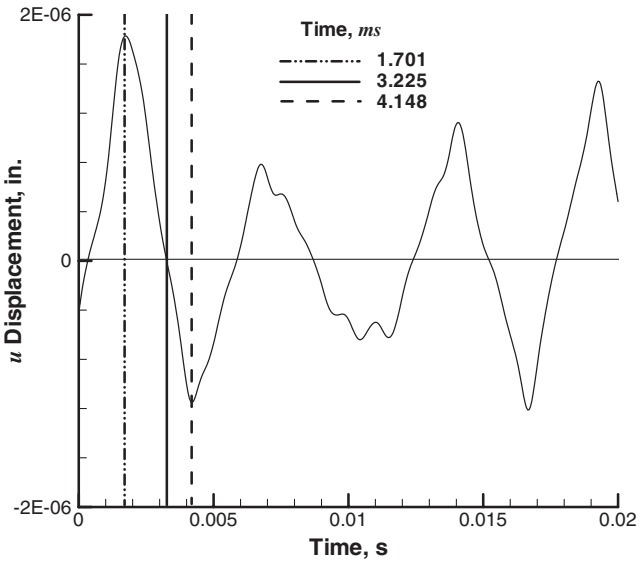

Fig. 7 Midspan horizontal displacement time history at 0.6517 lb/in. distributed loading.

utilized for all analyses. The element-by-element time step estimation uses a stability limit based on the highest element frequency in the whole model. The element-by-element time step estimate is therefore conservative and gives a smaller stable time increment than the true stability limit which is based upon the maximum frequency of the entire model [19]. A total time of 2.1384 s was simulated for each loading level considered and the first 0.5 s was removed to eliminate the transient response. The full-span ABAQUS model consisted of 144 B21 beam elements. All displacement results are presented in the global coordinate system as horizontal (u) and vertical (v) components.

The responses to four different excitation levels yielding slightly to highly nonlinear response characteristics were computed. The v and u displacement power spectral densities (PSDs) were examined at two locations, namely at the projected quarterspan of the arch (4.5 in. from the clamped boundary), presented in Figs. 2 and 3, and at the midspan (9.0 in. from the clamped boundary), presented in Figs. 4 and 5. Displacement responses at the quarterspan location (Figs. 2 and 3) clearly indicate a significant change in the PSD characteristics when passing from the 0.4608 to the 0.6517 lb/in. excitation level. In particular, the emergence of a peak at approximately 158 Hz is noted. At the midspan location, the v displacement PSD (Fig. 4) does not indicate this change in character. Examination of midspan u displacement PSD (Fig. 5), however, indicates negligible response amplitude at the 0.2304 lb/in. excitation level, followed by a significant jump in amplitude at and above the 0.6517 lb/in. excitation level. The 0.4608 lb/in. excitation level appears to produce a response in a transition region.

The jump in response in Fig. 5 was investigated in further detail. Figure 6 presents midspan u displacement time histories ranging from the 0.2304 to 1.3033 lb/in. excitation levels. At the excitation level of 0.2304 lb/in., the midspan u response is negligible. Previous work indicated this to be the case for a planar isotropic and uniformly loaded beam, regardless of the excitation level applied [8]. For the loading level of 0.6517 lb/in., the midspan u displacement of the arch exhibits intermittent damped transients. At the excitation level of 1.3033 lb/in., the motion is of a permanent nature. A few instantaneous snapshots of a full-field displacement along the span of the arch for the 0.6517 lb/in. loading were studied to determine the nature of this motion. Snapshots were chosen from the evolved u displacement time history shown in Fig. 7, such that the center point displacement was positive (left of the neutral position, $t = 1.701$ ms), negative (right of the neutral position,

$t = 4.148$ ms), and nearly zero (at the neutral position, $t = 3.225$ ms). Snapshots of the v and u displacements along the arch span for these three conditions are presented in Figs. 8 and 9, respectively. When the midspan u response is zero ($t = 3.225$ ms), the v displacement is symmetric and u displacement is antisymmetric. It is seen in both figures that symmetry of the v displacement response and antisymmetry of the u displacement response is only preserved when the midspan u displacement is zero. When the midspan u displacement response is positive ($t = 1.701$ ms), the v displacement response is no longer symmetric and its maximum occurs at approximately the quarterspan point from the right end. When the midspan u displacement response is negative ($t = 4.148$ ms), the v displacement response is also no longer symmetric, with its maximum at approximately the quarterspan point from the left end. These observations lead to the conclusion that both u and v displacements are generally a superposition of both symmetric and antisymmetric behaviors.

Because of the symmetry of the arch geometry and the loading distribution, it can also be concluded that there exists no direct form of excitation that would initiate the antisymmetric v and/or symmetric u displacement responses, i.e., nonsymmetric v displacement and/or any midspan u motion. Therefore, this behavior must be initiated by energy transfer from the primary system, which is consistent with the geometry and loading. Recalling Sec. I, such an observation fulfills a definition of an autoparametric resonance. The analysis in physical DoFs, however, is unable to provide detailed insight as to what modes contribute to the antisymmetric behavior. Certainly, inspection of Figs. 2 and 3 can provide some clues regarding the new frequency components introduced with the antisymmetric v displacement response (i.e., at approximately 160, 520, and 1070 Hz). However, since the response is nonlinear, characterization of this nonlinear behavior in terms of linear modes is appropriate only in the context of a nonlinear modal simulation.

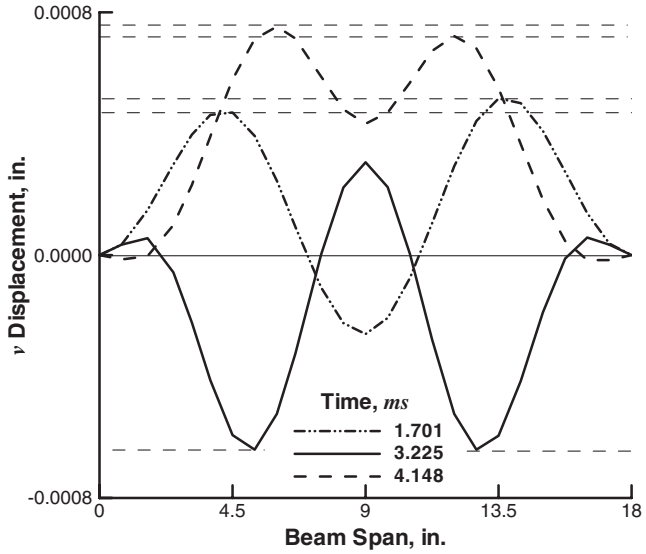

Fig. 8 Vertical displacement field for selected time instances at 0.6517 lb/in. distributed loading.

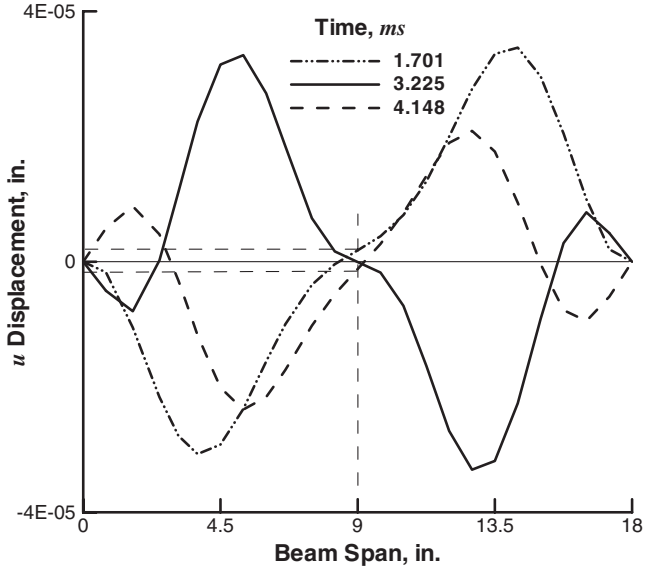

Fig. 9 Horizontal displacement field for selected time instances at 0.6517 lb/in. distributed loading.

Founded on experience built upon flat and isotropic thin-walled structures analysis, there exists a perception that a nonlinear analysis is generally an attempt to mitigate conservativeness or overdesign that would result from a linear analysis. However, nonlinear curved and/or anisotropic structural analysis can result in a solution that will not be upper-bounded by a linear analysis [13,14]. Figures 10 and 11 present linear and nonlinear vertical root mean square (RMS) displacement results at the midspan and quarterspan locations, respectively. It is clearly seen that for the shallow arch analyzed herein, the displacements at both selected locations obtained from the nonlinear analysis will exceed the results obtained from the linear calculations. Hence, this structure exhibits a spring softening nonlinearity and is nonconservative relative to the linear system.

III. Reduced Order Numerical Simulation

The nonlinear reduced order numerical simulation analysis consists of several parts [8]. The linear eigenvectors, commonly employed as basis functions, are first obtained from a commercial finite element program (in this study ABAQUS v.6.5-1). Following a transformation of the nonlinear system of equations to modal coordinates, the modal stiffness coefficients are evaluated and the resulting coupled system of equations is numerically integrated to obtain the modal displacement time history. The modal solution is transformed back to physical coordinates and can be postprocessed as desired. It should be pointed out that for the purpose of analyzing nonplanar structures, the formulation previously presented [7,8,11] has not been redeveloped. However, the guidelines for the selection of basis functions must be substantially revised.

A. Modal Coordinate Transformation

The equations of motion of the nonlinear system in physical DoFs may be written as

$$\boldsymbol{M}\ddot{\boldsymbol{X}}(t) + \boldsymbol{C}\dot{\boldsymbol{X}}(t) + \boldsymbol{F}_{NL}(\boldsymbol{X}(t)) = \boldsymbol{F}(t) \tag{1}$$

where $\boldsymbol{M}$ and $\boldsymbol{C}$ are the mass and proportional damping matrices, respectively, and $\boldsymbol{X}$ and $\boldsymbol{F}$ are the displacement response and force excitation vectors, respectively. The nonlinear restoring force $\boldsymbol{F}_{NL}$ contains the linear, quadratic, and cubic stiffness contributions.

A set of coupled modal equations with reduced degrees-of-freedom is first obtained by applying the modal coordinate transformation $\boldsymbol{X} = \boldsymbol{\Phi}\boldsymbol{q}$ to Eq. (1), where $\boldsymbol{q}$ is the modal displacement response vector. The modal basis function matrix $\boldsymbol{\Phi}$ is typically formed from the eigenvectors obtained from Eq. (1) using only the linear stiffness. Generally, a small set of L basis functions are included giving

$$\tilde{\boldsymbol{M}}\ddot{\boldsymbol{q}}(t) + \tilde{\boldsymbol{C}}\dot{\boldsymbol{q}}(t) + \tilde{\boldsymbol{F}}_{NL}(q_1(t), q_2(t), \ldots, q_L(t)) = \tilde{\boldsymbol{F}}(t) \tag{2}$$

where the tilde superscript represents modal quantities, and

$$\tilde{\boldsymbol{M}} = \boldsymbol{\Phi}^T\boldsymbol{M}\boldsymbol{\Phi} = \lceil \boldsymbol{I} \rfloor \qquad \tilde{\boldsymbol{C}} = \boldsymbol{\Phi}^T\boldsymbol{C}\boldsymbol{\Phi} = \lceil 2\zeta_r\omega_r \rfloor$$
$$\tilde{\boldsymbol{F}}_{NL} = \boldsymbol{\Phi}^T\boldsymbol{F}_{NL} \qquad \tilde{\boldsymbol{F}} = \boldsymbol{\Phi}^T\boldsymbol{F} \tag{3}$$

B. Indirect Stiffness Evaluation Method

The previously developed indirect stiffness evaluation method is applied [7,8,11]. To summarize, the rth component of the nonlinear

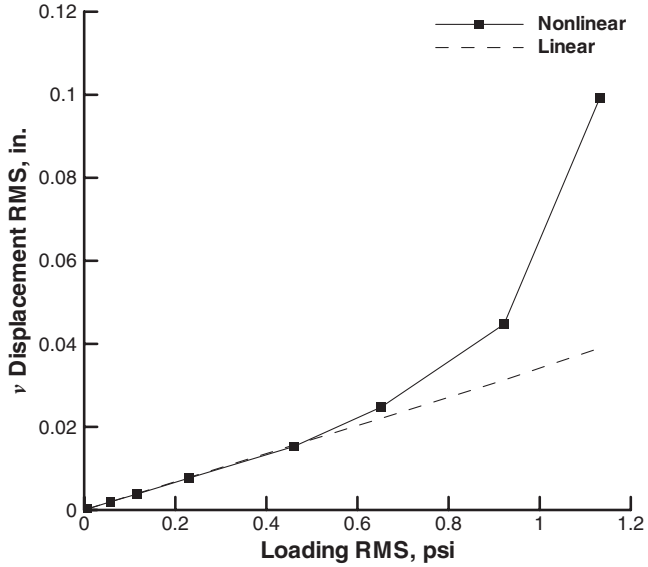

Fig. 10 Midspan v displacement RMS.

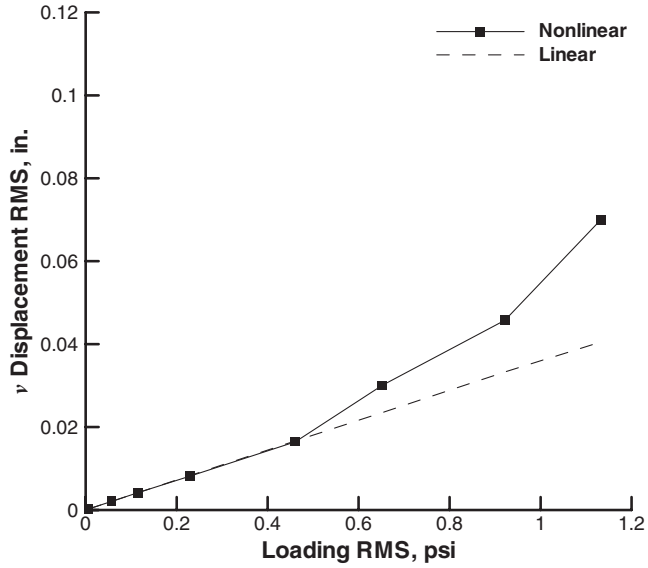

Fig. 11 Quarterspan v displacement RMS.

force vector in Eq. (2) may be written in the form

$$\tilde{F}^r_{NL}(q_1, q_2, \ldots, q_L) = \sum_{j=1}^{L} d^r_j q_j + \sum_{j=1}^{L}\sum_{k=j}^{L} a^r_{jk} q_j q_k + \sum_{j=1}^{L}\sum_{k=j}^{L}\sum_{l=k}^{L} b^r_{jkl} q_j q_k q_l \qquad r = 1, 2, \ldots, L \tag{4}$$

where d, a, and b are the linear, quadratic nonlinear, and cubic nonlinear modal stiffness coefficients, respectively. This form reduces the problem of determining the nonlinear stiffness from one in which a large set of simultaneous nonlinear equations must be solved to one involving simple algebraic relations. The algebraic relations are obtained by solving a series of nonlinear static problems with prescribed displacement fields [7,8,11]. Note that the indirect procedure, contrary to the direct methods [1–3,14], does not neglect in-plane inertia of the system.

C. Eigenanalysis

As mentioned briefly in Sec. III.A, a reduced order method usually employs a subset of selected eigenvectors as a set of basis functions to be used in a reduced order stiffness evaluation procedure. As expected and explained in Sec. I, the identification and classification of these eigenvectors for a shallow structure is more involved than for planar configurations. It is helpful to categorize the linear eigenvectors that constitute the modal basis by their symmetry. For the shallow arch under consideration, two categories are defined. Those having symmetric transverse displacements, with symmetric rotations and in-plane displacements, are subsequently referred to as ST modes. Those having antisymmetric transverse displacement, with symmetric rotations and in-plane displacements, are referred to as AT modes. Each eigenvector consists of both transverse and in-plane components, therefore, an additional criteria is needed in an attempt to recognize whether a particular mode will be contributing more to a transverse or in-plane response component. In this work, the following classification was adopted. For each mass-normalized eigenvector, the maximum transverse and in-plane components were determined. If the maximum transverse component was greater than the maximum in-plane component, the mode was classified as type T–*transverse dominated*. If the maximum in-plane component was greater than the maximum transverse component, the mode was classified as type I–*in-plane dominated*. Hence, four classes of modes are considered for inclusion in the modal basis, i.e., ST-T, ST-I, AT-T, and AT-I. Note that this scheme for classifying mode type is applicable only to the shallow curvatures under consideration here. For deeper curvatures, an alternative classification scheme would likely be necessary. It should also be noted that either the full-span model or a semispan model, analyzed with both symmetric and antisymmetric midspan boundary conditions, are needed to obtain the above suite of eigenvectors.

The identical full-span ABAQUS model was used for both the physical DoFs solution and eigenanalysis for the reduced order numerical simulation. Selected modes with their ordering numbers, corresponding natural frequencies, and the above-introduced classification are shown in Table 1. For the structure considered, type T modes typically have lower natural frequencies than type I modes. Vertical displacement, rotation, and horizontal displacement components of the lowest natural frequency eigenvectors of each of the four categories defined above are shown in Figs. 12–15.

At this point, it is also worthwhile to note that the concept of so-called companion [10] or dual [11,12] modes developed for planar structures is no longer needed nor relevant. These bases were previously introduced to obtain membrane behavior corresponding to bending modes of flat structures. Since the modes are linearly coupled for curved structures, these degrees-of-freedom are automatically reflected in the basis.

D. Modal Stiffness Relationships

It was previously shown [8] that the linear modal stiffness obtained from the indirect stiffness evaluation method is equivalent to that obtained via a standard modal analysis, that is,

Table 1 Natural modes: classification and frequencies

Mode designator	Mode number	Frequency, Hz
ST-T_1	2	258.17
ST-T_2	3	400.41
ST-T_3	5	773.72
ST-T_4	7	1426.0
ST-I_1	22	11,225
ST-I_2	33	22,437
ST-I_3	42	33,638
ST-I_4	51	44,826
AT-T_1	1	158.25
AT-T_2	4	513.19
AT-T_3	6	1070.1
AT-T_4	8	1828.0
AT-I_1	15	5624.3
AT-I_2	28	16,831
AT-I_3	38	28,039
AT-I_4	47	39,235

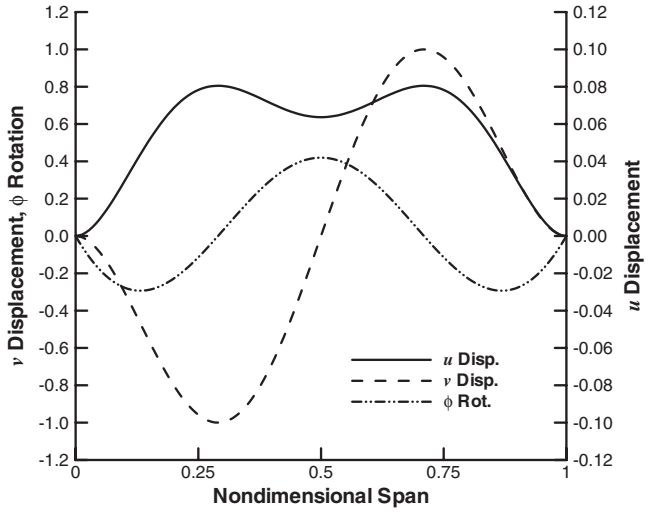

Fig. 12 The first type T antisymmetric transverse mode AT-T_1 (158 Hz).

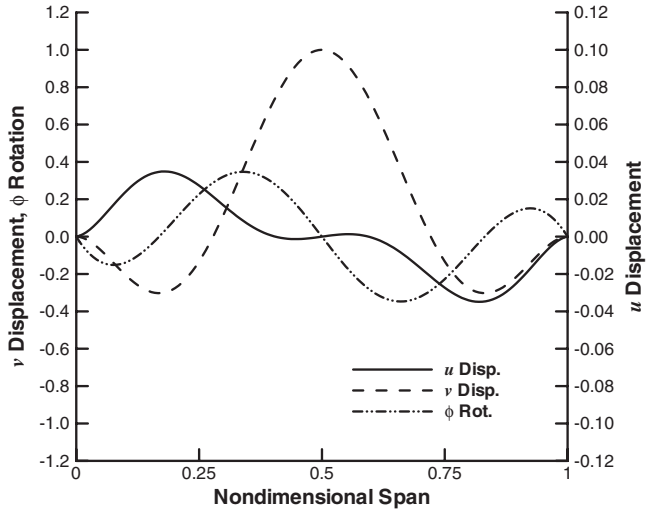

Fig. 13 The first type T symmetric transverse mode ST-T_1 (258 Hz).

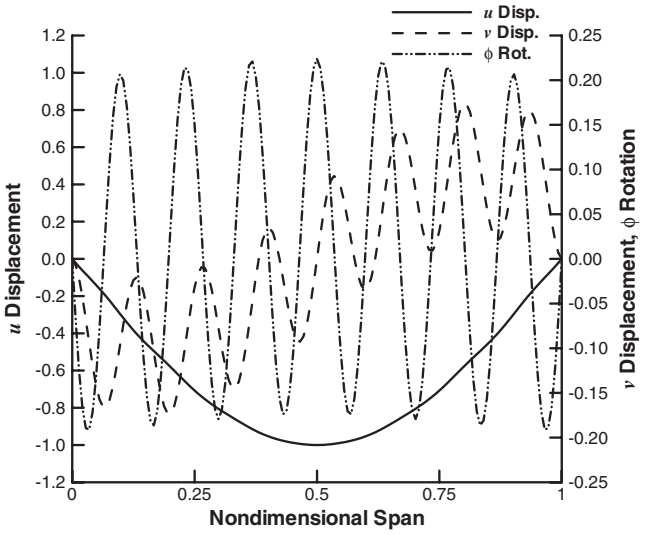

Fig. 14 The first type I antisymmetric transverse mode AT-I_1 (5.6 kHz).

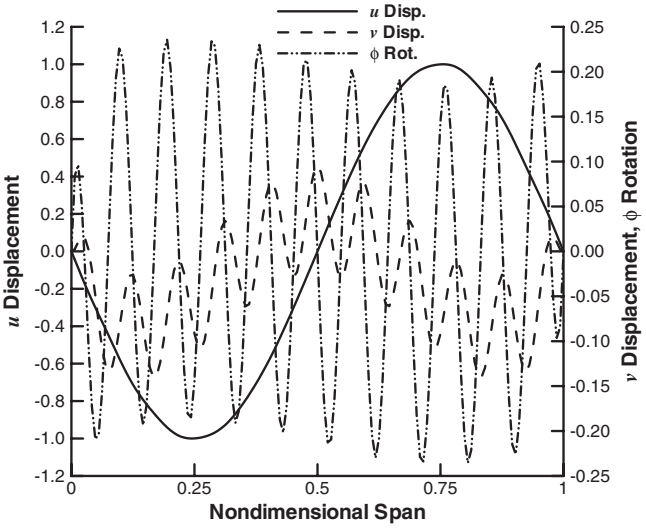

Fig. 15 The first type I symmetric transverse mode ST-I_1 (11.2 kHz).

$$\boldsymbol{d} = \tilde{\boldsymbol{K}} = \boldsymbol{\Phi}^T \boldsymbol{K} \boldsymbol{\Phi} = \lceil \omega_r^2 \rfloor \tag{5}$$

As expected, there is zero modal coupling through the linear modal stiffness. Additionally, certain relationships exist between significant quadratic and cubic nonlinear stiffness terms [7,8]. For the quadratic terms, these are

$$a_{12}^1 = 2a_{11}^2 \qquad 2a_{22}^1 = a_{12}^2 \tag{6}$$

For the cubic terms, these are

$$b_{122}^1 = b_{112}^2 \qquad 3b_{222}^1 = b_{122}^2 \qquad 3b_{111}^2 = b_{112}^1 \tag{7}$$

Without citing particular values, these relationships are maintained for the present problem.

An inspection of the nonlinear modal stiffness coefficients can be helpful to reveal couplings that may exist between specific types of bases. In the following, it should be recognized that signs of the modal nonlinear stiffness coefficients are only affected by signs of the utilized basis functions (in this case, eigenvectors), which are not unique, and by signs of scaling factors applied to them, which are also arbitrary. Therefore, the absolute value of coefficients will be used to identify coupling of modes. Since the quadratic stiffness matrix is three-dimensional and the cubic stiffness matrix is four-dimensional, a spot inspection of numerical values may not be particularly revealing. Thus, a graphical representation is offered herein.

Figure 16 presents the absolute values of quadratic stiffness coefficients a_{jk}^i for the basis formed out of four AT-T, four ST-T, four AT-I, and four ST-I bases, that is, AT-T_{1-4}, ST-T_{1-4}, AT-I_{1-4}, ST-I_{1-4}. These bases are numbered from 1–16, e.g., basis 15 refers to ST-I_3. The basis selection is discussed in the next section. Each of the 16 subplots has index i fixed, and indices j and k are shown on the horizontal and vertical axes of each subplot, respectively. The scale bar indicates the coupling strength, with darkest cells effectively depicting a lack of coupling between the basis functions involved.[‡‡] It is seen that similar coupling patterns between three modes are indicated for each row of subplots. For example, the top row shows strong coupling between AT-T modes ($1 < i < 4$), AT-T modes ($1 < j < 4$), and ST-I modes ($13 < k < 16$), and also between AT-T modes ($1 < i < 4$), ST-T modes ($5 < j < 8$), and AT-I modes ($9 < k < 12$). The remaining rows indicate different couplings between three modes.

As mentioned before, the cubic matrix is four-dimensional, and so a two-dimensional graphical representation of coefficients b_{jkl}^i requires fixing of two indices, say i and j, and varying the remaining

[‡]A version of this paper with full-color artwork is available online in electronic form.

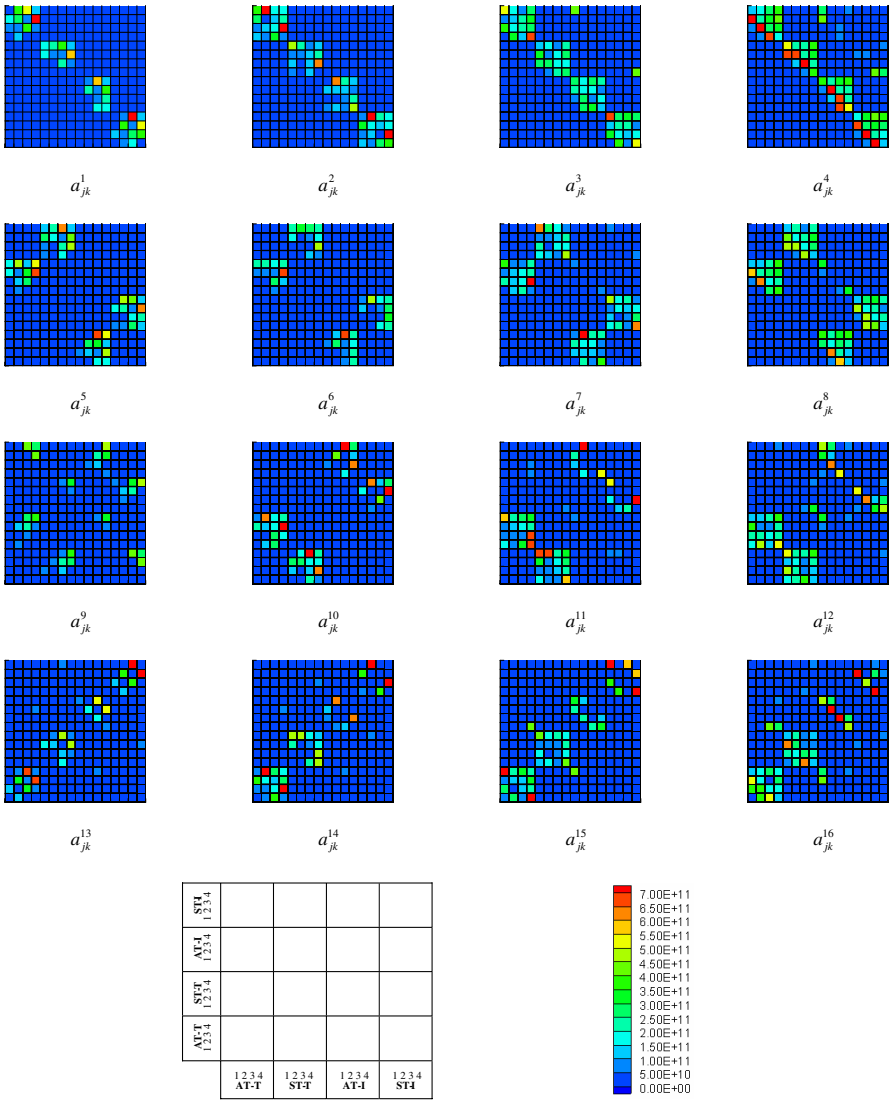

Fig. 16 Quadratic nonlinear modal stiffness coefficients.

two, k and l, on the horizontal and vertical axes, respectively. For 16 bases, this procedure would produce 256 two-dimensional plots. However, the same trend as previously found for the quadratic matrix was also observed for the cubic matrix, namely, when indices i and j each vary within the same type of basis function, the couplings resemble very similar patterns. For example, for an i-index variation within the AT-T basis ($1 < i < 4$), and a j-index variation within the ST-T basis ($5 < j < 8$), plots corresponding to any of coefficients $b^{1-4}_{5-8\ k\ l}$, are similar. Thus, the cubic modal stiffness coefficients can be represented in 16 subplots, as shown in Fig. 17. Each subplot indicates different couplings between four modes and is representative of 16 such subplots.

The specific conclusion to be drawn based on Figs. 16 and 17 is that not all possible means of coupling are exercised in the particular problem under investigation. At the same time, it is observed that none of the basis subsets utilized in the analysis is completely uncoupled from the rest of the basis functions. For example, for the cubic modal stiffness $b^{1}_{12\ 13-16\ 13-16}$, the coupling between AT-T, AT-I, ST-I, and ST-I modes is effectively zero (see $b^{1}_{12\ k\ l}$ in Fig. 17). However, a different combination of these same three mode types is coupled by means of the cubic modal stiffness $b^{13}_{16\ 9-12\ 1-4}$ (modes ST-I, ST-I, AT-I, and AT-T, see $b^{13}_{16\ k\ l}$ in Fig. 17).

In general, it is not possible to determine whether the selected set of basis functions is insufficient from the modal coupling plots. However, it is possible to determine which modes would not contribute to the response. If a specific mode is completely uncoupled from the rest of the basis, and also is not directly excited, then its presence in the basis would not be necessary. The detailed assessment of the basis set sufficiency is reserved for the following section. This assessment is based on reconstructed physical displacements following computation of the modal response in a process which involves modal summation.

E. Reduced Order Analysis Results

For the shallow curvature considered, two factors affected the initial modal basis selection. The first was earlier experience with symmetric planar structures under symmetric transverse loadings where the initial basis consisted of low frequency bending modes [7–12]. For the curved configuration, an analogous basis consisting of transverse component dominated (type T) modes was chosen. Like the earlier experience, the addition of higher frequency in-plane dominated modes (type I) was expected to improve the prediction of peak magnitudes and their broadening in a highly nonlinear regime [8]. The second selection factor was based on observations made through the simulation in physical DoFs. There, the need for both ST-T and AT-T modes was indicated for autoparametric resonance conditions. Because the presence of both type T modes was indicated, both type I modes were also included to improve the prediction. Thus, the modal bases considered consisted of all four types of modes. In the following, an abbreviated convention describing the set of modes applied in a particular analysis was used. The convention consists of a four-digit sequence containing the number of included ST-T, ST-I, AT-T, and AT-I modes, in that order. Note that this ordering is not based on modal frequency and, hence,

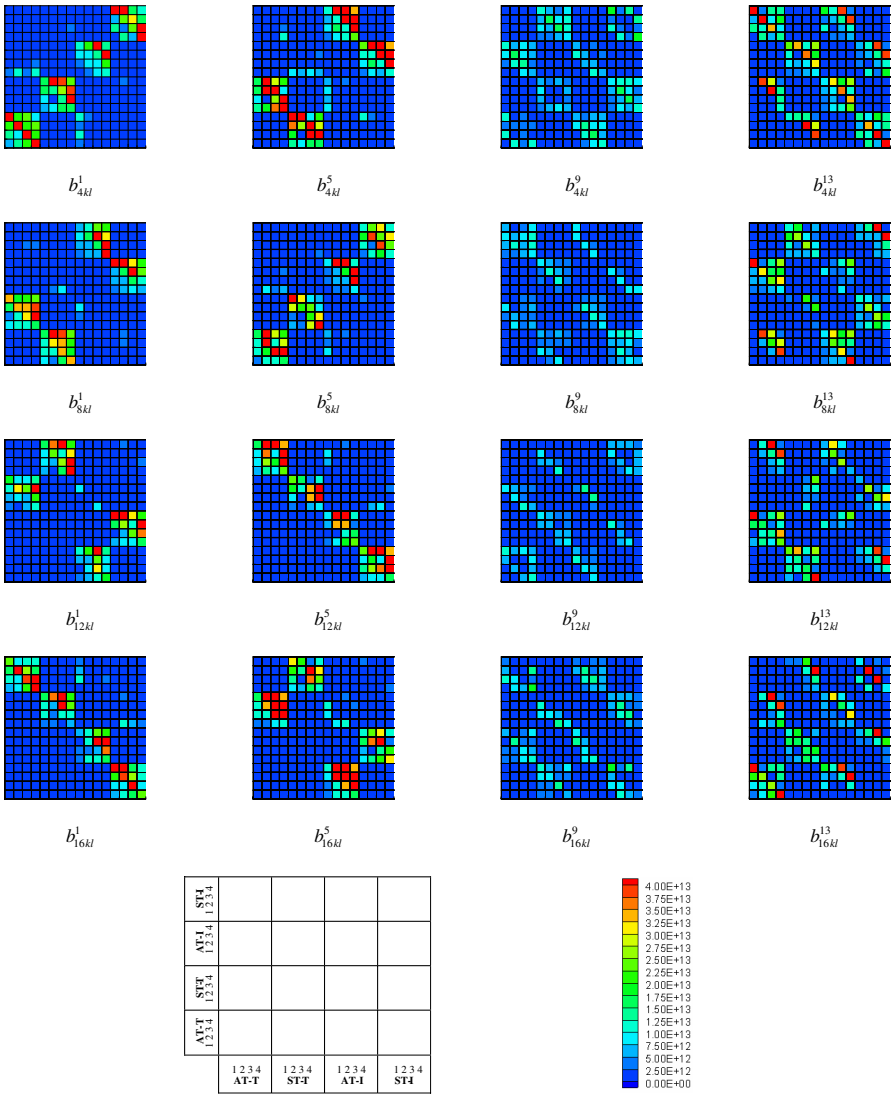

Fig. 17 Cubic nonlinear modal stiffness coefficients.

differs from that of Figs. 16 and 17. For example, 4044 indicates a basis consisting of four ST-T, zero ST-I, four AT-T, and four AT-I modes.

Two excitation levels were selected for investigation: 0.2304 lb/in. was shown to give rise to a slightly nonlinear response, and 0.6517 lb/in. produced a highly nonlinear response. As illustrated in Fig. 6, the lower excitation level does not produce an autoparametric response, whereas the higher level produces an intermittent autoparametric behavior. For both loading levels, the following suite of basis functions was considered. The 4040 basis was selected as the baseline as it contained only type T modes, i.e., four ST-T and four AT-T modes. The 4440 basis was used to determine the effect of ST-I modes on the baseline. Similarly, the 4044 basis was used to determine the effect of AT-I modes on the baseline. The effect of both types of in-plane dominated modes on the baseline was studied using the 4444 basis. Two additional bases were considered to investigate the contribution of only ST-T modes in the 4000 basis, and the contribution of only AT-T modes, in the 0040 basis. These last two bases were ideal for investigating the response to direct excitation. The ability to interrogate the nonlinear response in this manner is a unique capability of the nonlinear modal simulation. An analysis in physical DoFs can only approximate this ability by limiting the frequency bandwidth of the excitation field. The effect of nonlinear modal coupling, however, remains in that case.

Having the nonlinear force vector in Eq. (4) fully defined with any set of the basis functions described previously, the coupled modal nonlinear equations of motion given by Eq. (2) were numerically integrated using a fourth-order Runge–Kutta method [20]. Consistent with the analysis in physical DoFs, a total time of 2.1384 s was simulated and the initial 0.5 s of transient response was removed. A fixed time integration step of 2 μs was used. The resulting modal displacement time histories were transformed back to physical coordinates using the inverse modal transformation.

Horizontal and vertical displacement PSDs obtained via reduced order analysis were compared with those obtained via the analysis in physical DoFs at two locations along the span of the arch, namely at the center and quarterspan nodes. The need to select more than one validation point was based on the observation from the analysis in physical DoFs that the change in nonlinear response manifests itself in different ways at different locations. At the quarterspan location, the emergence of an additional peak was noted in Figs. 2 and 3. At the midspan node, the u displacement component exhibited a sudden jump in response level with the onset of autoparametric resonance.

Figures 18–20 present the comparison of the reduced order solutions obtained with different bases and the solution in physical DoFs at the 0.2304 lb/in. excitation level. For these and subsequent plots, significant peaks are annotated with their corresponding modal component to aid the discussion. It should be understood that these annotations do not imply the presence of linear modes in the nonlinear response. The u displacement at the midspan is not shown because all analyses yielded numerical zero. All reduced order displacement PSDs compare well with the physical DoFs solution and demonstrate behaviors due solely to ST modes. This is evidenced

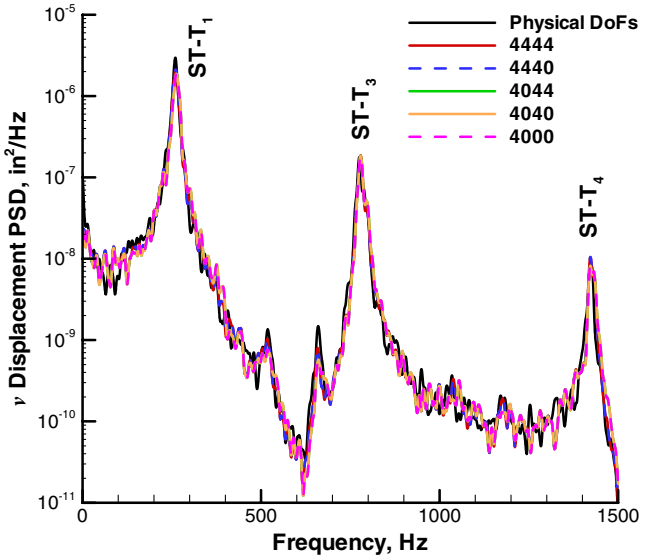

Fig. 18 Midspan vertical displacement at 0.2304 lb/in. distributed loading.

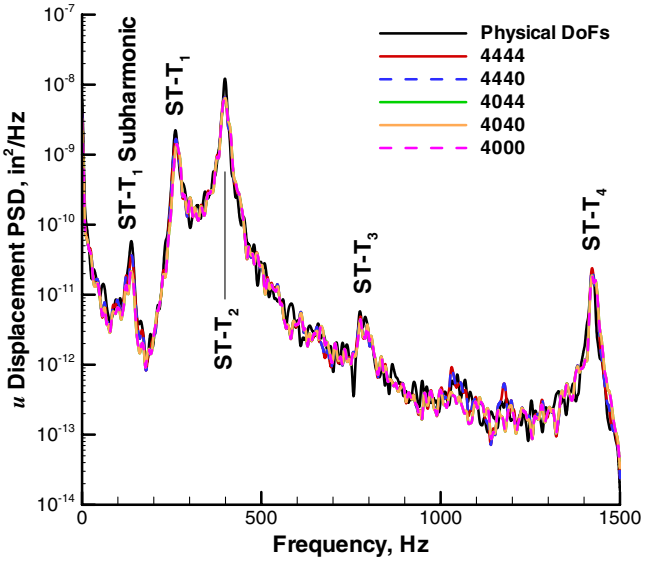

Fig. 20 Quarterspan horizontal displacement at 0.2304 lb/in. distributed loading.

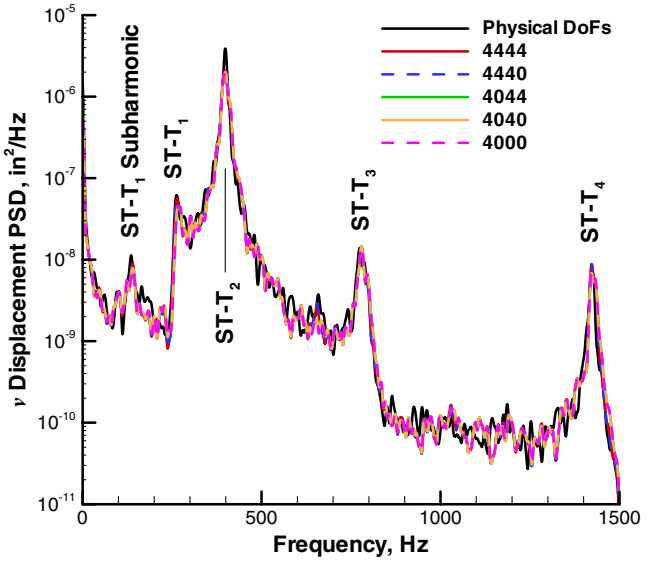

Fig. 19 Quarterspan vertical displacement at 0.2304 lb/in. distributed loading.

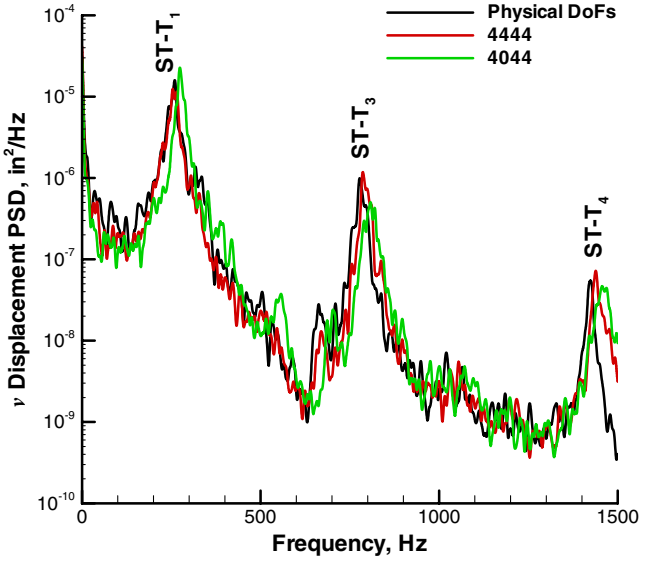

Fig. 21 Midspan vertical displacement at 0.6517 lb/in. distributed loading.

by the fact that the inclusion of AT-T and AT-I modes in the basis do not alter the computed response, e.g., compare 4000 with 4040 and 4044. In fact, the 0040 basis resulted in a numerically zero response at both locations for both response components, indicating that the AT modes are not directly excited by the externally applied loading. The only noticeable difference between modal bases is apparent at the quarterspan location in the first subharmonic of the lowest ST-T mode (133 Hz). Upon close inspection, it is seen that the behavior is represented slightly better with the 44xx bases (4444 and 4440), than it is with any of the 40xx bases (4044, 4040, and 4000). Therefore, even for this slightly nonlinear response regime, the inclusion of ST-I modes is shown to improve the behavior related to the ST-T modal response. As evidenced by Figs. 16 and 17 introduced in Section III. D, this is due to the presence of cross coupling of nonlinear stiffness terms, in this case between the ST-T and ST-I mode pairs (see $a_{j\ k}^{5-8}$ in Fig. 16, and $b_{12\ k\ l}^{1}$ and $b_{16\ k\ l}^{5}$ in Fig. 17, for example). Note that if the excitation bandwidth were sufficiently increased, the ST-I modes would also be directly excited. From this load level, we conclude that the ST-T modes (through direct excitation) and ST-I modes (through coupling with ST-T modes) constitute the primary system.

Figures 21–28 show the results obtained at an excitation level of 0.6517 lb/in.. For clarity, each set of solutions is displayed in two separate figures. One figure indicates the physical DoFs, 4444, and 4044 solutions. The second figure shows the physical DoFs, 4440, 4040, and 4000 solutions.

At the midspan location, the v displacement response (Figs. 21 and 22) is dominated by the peak originating from the first ST-T mode. The response is best modeled by the 4444 and 4440 bases. Because the PSD response does not indicate a presence of peaks originating from anything other than ST-T modes, this result is found consistent with the conclusions based on 0.2304 lb/in. case, where the comparison of 44xx bases with the physical DoFs solution was found superior to the 40xx bases. The 40xx bases (4044, 4040, and 4000) overpredict the degree of nonlinearity. This is evidenced through excessive stiffening (peaks moved to the higher frequencies compared with physical DoFs) of the first, third, and fourth ST-T-related peaks and excessive broadening, especially of the fourth peak. The second ST-T-related behavior is not significantly present at this location. The solution for the 0040 basis was numerically zero, indicating that the AT-T modes were not directly excited.

Midspan u displacement results (Figs. 23 and 24) offer a different perspective. The response exhibits peaks originating from the AT-T modes. The 0040 basis yielded a numerically zero response, again indicating that the AT-T modes are not directly excited by the

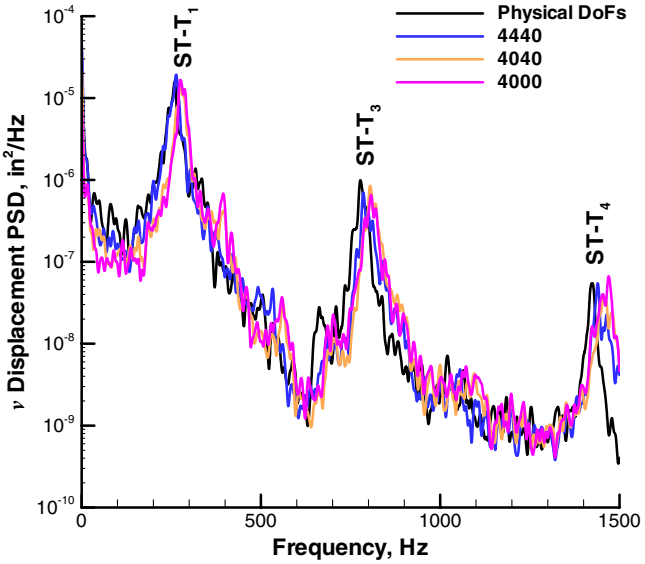

Fig. 22 Midspan vertical displacement at 0.6517 lb/in. distributed loading.

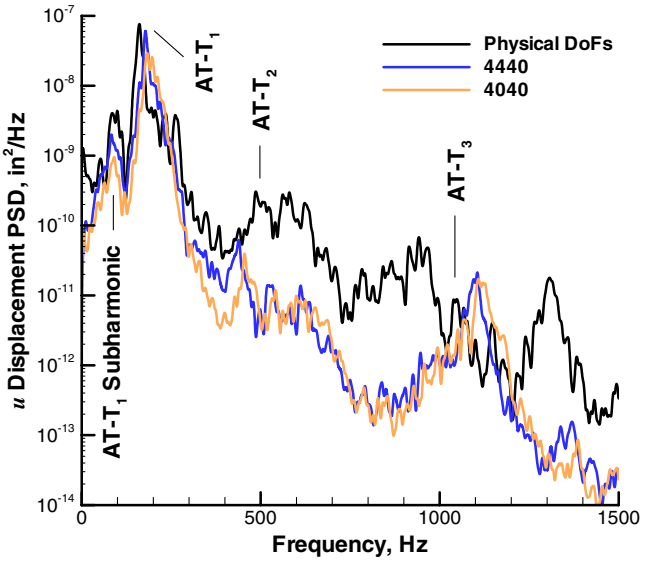

Fig. 24 Midspan horizontal displacement at 0.6517 lb/in. distributed loading.

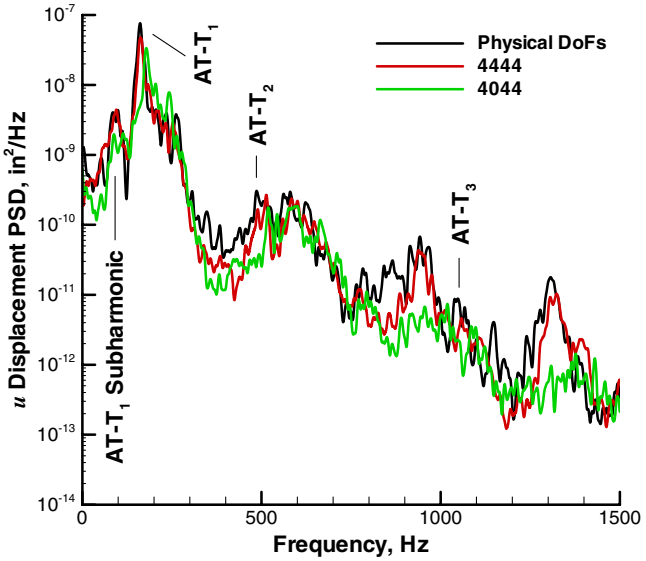

Fig. 23 Midspan horizontal displacement at 0.6517 lb/in. distributed loading.

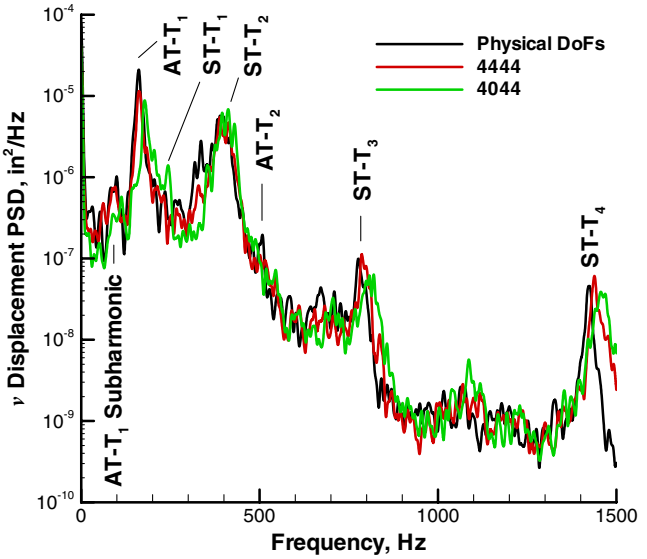

Fig. 25 Quarterspan vertical displacement at 0.6517 lb/in. distributed loading.

externally applied loading. The excitation provided to the AT-T modes is therefore applied indirectly through autoparametric resonance. Thus, the AT-T modes (through autoparametric resonance) and the AT-I modes (through coupling with the AT-T modes) constitute the secondary system. The modal bases containing ST and both AT-T and AT-I modes are therefore expected to correspond best with the physical DoFs solution for this condition. The solution for basis 4044, shown in Fig. 23, corresponds fairly well with the physical DoFs solution. However, the magnitude of the first AT-T peak is too low and it demonstrates overstiffening. Further, the comparison beyond approximately 750 Hz frequency range is deficient. The addition of ST-I modes in basis 4444 activates the ST-T to ST-I coupling and improves the comparison throughout the frequency range. Bases which do not include AT-I modes (4440 and 4040) suffer as the AT-T to AT-I coupling is not represented, see Fig. 24. The 4440 basis captures the behavior of the first AT-T peak better than the 4040 basis, likely due to the ST-T to ST-I coupling. Beyond about 300 Hz, both 4440 and 4040 bases compare poorly, as the response level generally underpredicts the physical DoFs solution except in the frequency range between 1050 and 1200 Hz, where the contribution of the third AT-T is exaggerated. It can be concluded that the higher frequency modes of both kinds, ST-I and AT-I, are needed for an accurate midspan horizontal displacement prediction when the structure undergoes autoparametric resonance. However, inclusion of the AT-I modes is more important than inclusion of the ST-I modes, as evidenced by the improved comparison of the 4044 basis relative to the comparison of the 4440 basis. This observation further substantiates the importance of the coupling between the ST-T and ST-I modes (as indicated previously) and between the AT-T and AT-I modes (see $a_{j\ k}^{5-8}$ in Fig. 16 and $b_{12\ k\ l}^{1}$ and $b_{16\ k\ l}^{5}$ in Fig. 17, for example). Note that basis 4000 resulted in an essentially zero horizontal displacement response, indicating that the basis is incapable of representing the secondary system and capturing the autoparametric interactions.

At the quarterspan location, the v displacement component (Figs. 25 and 26) is best captured by basis 4444. Basis 4000 does not have means of representing the antisymmetric behavior and consequently provides a solution that fails to capture the behavior of the secondary system. This is particularly apparent in the lack of the peak originating from the first AT-T mode, including its subharmonic peak. Among those bases that are capable of reflecting the antisymmetric behavior, basis 4040 is of the lowest quality. It

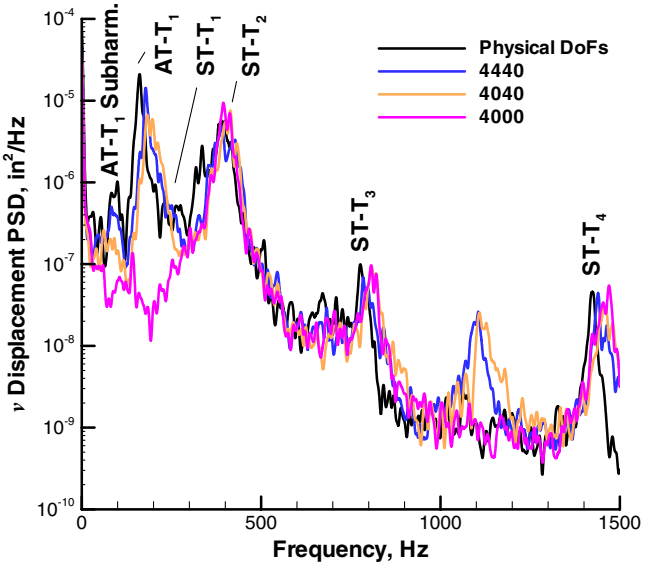

Fig. 26 Quarterspan vertical displacement at 0.6517 lb/in. distributed loading.

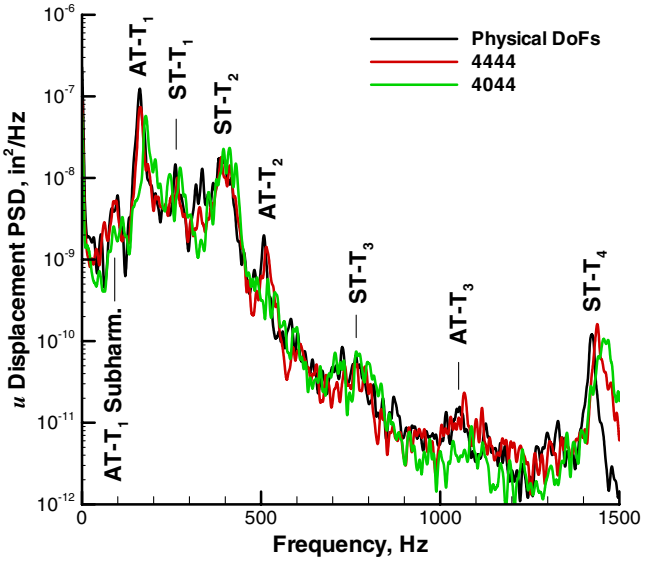

Fig. 27 Quarterspan horizontal displacement at 0.6517 lb/in. distributed loading.

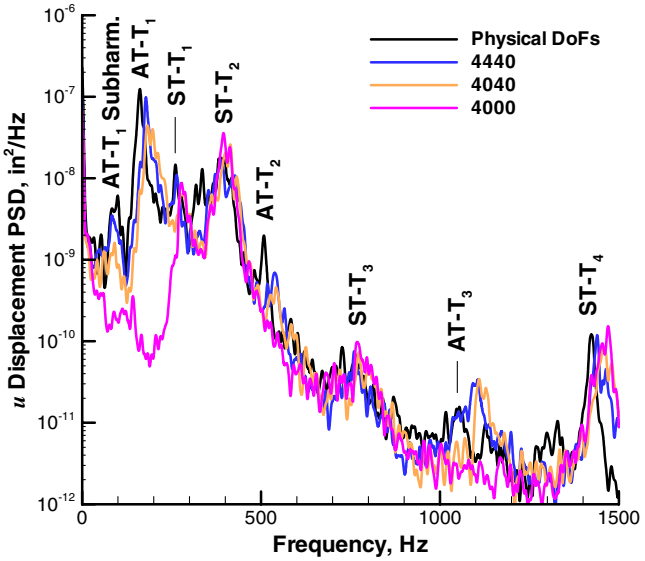

Fig. 28 Quarterspan horizontal displacement at 0.6517 lb/in. distributed loading.

poorly represents the peak originating from the first AT-T mode in that it is overstiff (its peak magnitude is too small and is shifted toward higher frequency). Additionally, its AT-T subharmonic is too small, whereas the contribution of the third AT-T mode is exaggerated. The quality of solutions from bases 4440 and 4044 consistently falls between the best (4444) and the worst (4040). Overall, basis 4440 matches the peak magnitudes and broadening better than the 4044 basis. The exception is in the frequency range related to the third AT-T mode (approximately 1050–1150 Hz), in which the solution from the 4440 basis is vastly exaggerated, whereas the solution from the 4044 basis overpredicts this peak only slightly.

At the quarterspan, the u displacement component (Figs. 27 and 28) obtained with 4444 basis is again superior to all the others. It very accurately matches peaks originating from both the ST-T and AT-T modes. It is particularly worthwhile to note that the 4444 basis is the only one that does not exhibit overstiffening of the first AT-T related peak and accurately captures the second and the third AT-T related peaks. Remarks made regarding the performance of 4440, 4040, and 4000 solutions for the vertical displacement component apply to the horizontal displacement component as well. The only exception is that the 4044 basis underpredicts the peak originating from the third AT-T mode for the u displacement component.

IV. Conclusions

The effect of modal basis selection on the displacement response predicted using a nonlinear modal simulation was investigated. For the shallow arch considered, it was found that

1) At a sufficiently high excitation level, autoparametric resonance can exist.

2) For a symmetric curved structure and symmetric loading distribution, the primary system consists of ST-T and ST-I modes and these modes may be directly excited by external loadings with sufficient bandwidth.

3) For a symmetric curved structure and symmetric loading, modes AT-T and AT-I are never directly excited (regardless of the excitation level and bandwidth); these modes constitute the secondary system and are only indirectly excited through the nonlinear modal interactions at a sufficiently high response regime.

4) For nonplanar symmetric structures which may exhibit autoparametric resonance, the inclusion of both ST-T and AT-T modes is the necessary minimum to represent directly and indirectly loaded components.

5) Higher frequency mode variants (ST-I and AT-I) provide a significant enhancement of the solution quality in the highly nonlinear/autoparametric regime; for all the cases studied at the high excitation level, inclusion of all mode variants (ST-T, ST-I, AT-T, and AT-I) always provided the solution that compared best with the physical DoFs analysis.

6) The inclusion of all mode variants at any location or excitation level does not adversely affect the response prediction; when mode identification is difficult, it should be always "safe" to expand the set of basis functions.

7) In the highly nonlinear/autoparametric regime, modes ST-I appear to enhance ST-T-originating response features, whereas AT-I appear to enhance AT-T-originating response features; therefore, modal pairs ST-T with ST-I and AT-T with AT-I exhibit a strong coupling.

8) Validation of a reduced order solution vs physical DoFs analysis and/or experimental results should be performed at more than one location on the structure and/or by inspection of more than one response component, as some of the locations may coincide with nodal points of the modes involved; e.g., if only transverse deflection at the center point would be considered, basis 4000 might have appeared sufficient.

9) Reliable evaluation of the quality of the solution as a function of modal truncation is difficult during the intermediate steps of the analysis in modal coordinates (i.e., based on modal stiffness coefficients); an accurate assessment can only be provided following the modal response computation and inverse transformation to physical DoFs.

10) Nonlinear analysis of shallow curvature structures may yield nonconservative results when compared with linear analysis.

11) The ability to interrogate the nonlinear response by altering the modal basis is a unique capability of the nonlinear modal simulation; analyses in physical DoFs will always reflect nonlinear modal coupling.

The results presented in this paper were for a particular shallow curvature. A possible area for future work is to determine the onset of autoparametric resonance as a function of curvature. A related interest is to extend the assessment of modal basis selection to structures having greater curvature and to those having linear coupling due to material anisotropy. At a minimum, it is expected that the present modal classification scheme would need modification for these cases.

References

[1] Mei, C., Dhainaut, J. M., Duan, B., Spottswood, S. M., and Wolfe, H. F., "Nonlinear Random Response of Composite Panels in an Elevated Thermal Environment," Air Force Research Lab. AFRL-VA-WP-TR-2000-3049, Wright–Patterson AFB, OH, Oct. 2000.

[2] Przekop, A., Guo, X., Azzouz, M. S., and Mei, C., "Reinvestigation of Nonlinear Random Response of Shallow Shells Using Finite Element Modal Formulation," AIAA Paper 2004-1553, 2004.

[3] Przekop, A., "Nonlinear Response and Fatigue Estimation of Aerospace Curved Surface Panels to Combined Acoustic and Thermal Loads," Ph.D. Dissertation, Old Dominion Univ., Norfolk, VA 2003.

[4] Ribeiro, P., "Modal Interactions in Shallow Arches," *Proceedings of the 7th International Conference on Computational Structures Technology*, edited by B. H. V. Topping, and C. A. Soares, Civil-Comp Press, Stirling, Scotland, 2004, pp. 177–178.

[5] Bathe, K. J., and Gracewski, S., "On Nonlinear Dynamic Analysis Using Substructuring and Mode Superposition," *Computers and Structures*, Vol. 13, No. 5–6, Oct.–Dec. 1981, pp. 699–707.

[6] McEwan, M. I., Wright, J. R., Cooper, J. E., and Leung, Y. T., "A Finite Element/Modal Technique for Nonlinear Plate and Stiffened Panel Response Prediction," AIAA Paper 2001-1595, 2001.

[7] Muravyov, A. A., and Rizzi, S. A., "Determination of Nonlinear Stiffness with Application to Random Vibration of Geometrically Nonlinear Structures," *Computers and Structures*, Vol. 81, No. 15, 2003, pp. 1513–1523.

[8] Rizzi, S. A., and Przekop, A., "The Effect of Basis Selection on Static and Random Response Prediction Using Nonlinear Modal Simulation," NASA TP-2005-213943, NASA Langley Research Center, Hampton, VA, Dec. 2005.

[9] Rizzi, S. A., and Muravyov, A. A., "Comparison of Nonlinear Random Response Using Equivalent Linearization and Numerical Simulation," *Structural Dynamics. Recent Advances, Proceedings of the 7th International Conference*, edited by N. S. Ferguson, H. F. Wolfe, M. A. Ferman, and S. A. Rizzi, Vol. 2, Inst. of Sound and Vibration Research, Univ. of Southampton, Southampton, UK, 2000, pp. 833–846.

[10] Hollkamp, J. J., Gordon, R. W., and Spottswood, S. M., "Nonlinear Sonic Fatigue Response Prediction from Finite Element Modal Models: a Comparison with Experiments," AIAA Paper 2003-1709, 2003.

[11] Mignolet, M. P., Radu, A. G., and Gao, X., "Validation of Reduced Order Modeling for the Prediction of the Response and Fatigue Life of Panels Subjected to Thermo-Acoustic Effects," *Structural Dynamics: Recent Advances, Proceedings of the 8th International Conference*, edited by M. J. Brennan, M. A. Ferman, B. A. T. Peterson, S. A. Rizzi, and K. Wentz, Inst. of Sound and Vibration Research, Univ. of Southampton, Southampton, UK, 2003.

[12] Radu, A. G., Yang, B., Kim, K., and Mignolet, M. P., "Prediction of the Dynamic Response and Fatigue Life of Panels Subjected to Thermo-Acoustic Loading," AIAA 2004-1557, 2004.

[13] Kobayashi, Y., and Leissa, A. W., "Large Amplitude Free Vibration of Thick Shallow Shells Supported by Shear Diaphragms," *Journal of Nonlinear Mechanics*, Vol. 30, No. 1, 1995, pp. 57–66.

[14] Przekop, A., Azzouz, M. S., Guo, X., Mei, C., and Azrar, L., "Finite Element Multiple-Mode Approach to Nonlinear Free Vibrations of Shallow Shells," *AIAA Journal*, Vol. 42, No. 11, 2004, pp. 2373–2381.

[15] Tondl, A., Ruijgrok, T., Verhulst, F., and Nabergoj, R., *Autoparametric Resonance in Mechanical Systems*, Cambridge Univ. Press, Cambridge, UK, 2000.

[16] Nayfeh, A. H., and Mook, D. T., *Nonlinear Oscillations*, Wiley, New York, 1995.

[17] Ibrahim, R. A., *Parametric Random Vibration*, Wiley, New York, 1985.

[18] Matthew, C., *Introduction to Linear, Parametric, and Nonlinear Vibrations*, Chapman and Hall, New York, 1990.

[19] ABAQUS version 6.5 On-line Documentation, ABAQUS Analysis User's Manual, Section 6.3.3, Abaqus, Providence, RI, 2005.

[20] Press, W. H., Teukolsky, S. A., Vetterling, W. T., and Flannery, B. P., "Numerical Recipes, the Art of Scientific Computing," [CD-ROM v2.10], Cambridge Univ. Press, Cambridge, UK, 2002.

S. Saigal
Associate Editor